Pak. J. Bot., 57(2): DOI: http://dx.doi.org/10.30848/PJB2025-2(34)

COMPARISON OF ANTIMICROBIAL, ANTICANCER AND ANTIOXIDANT PROPERTIES OF Fe, Cu, Ag NANOPARTICLES SYNTHESIZED FROM *SALVIA OFFICINALIS* PLANT

ESRA BALKIS[1], MURAT POLAT[1] AND BULENT KAYA[1*]

[1]*Institute of Sciences Bingöl University, Faculty of Arts and Sciences, Department of Molecular Biology and Genetics, Bingöl-12000 Turkey*
**Corresponding author's bkaya@bingol.edu.tr*

Abstract

The goal of this study was to comparatively investigate the physicochemical and biological activities of nanoparticles (NPs) formed by the reduction of *Salvia officinalis* (*S. officinalis*) using iron (Fe), copper (Cu), silver (Ag) metal salts. Fe@NPs, Cu@NPs, Ag@NPs *S. officinalis* leaves were synthesized using silver nitrate ($AgNO_3$), copper (II) sulfate ($CuSO_4$), ferric chloride ($FeCl_2$), ($FeCl_3$). Physical-morphological properties of NPs were determined using instrumental analysis techniques FT-IR, UV-visible, SEM, TEM, EDX, XRD and Zeta potential analysis. The antibacterial activity of NPs was evaluated by the disk diffusion method. Total antioxidant, total flavonoid/phenolic capacity, DPPH scavenging activity, metal chelating activities of NPs were also examined. Cytotoxic activity of NPs on A549 lung cancer cell lines was determined *in-vitro* by WST-1 assay. Fe@NPs 270-290, Cu@NPs 270-320, Ag@NPs 300-400 nm generated strong surface plasmon resonance in the range. According to SEM/TEM results show that Fe@NPs are round-cubic 49.3; Global 30.24 of Cu@NPs; showed that Ag@NPs had circular dimensions of 5,36 nm. Zeta potential values were determined as Fe@NPs -22.2, Cu@NPs 25.5, Ag@NPs -24.6 mV. As a result of antimicrobial analysis, the highest effect was seen in Ag@NPs. Synergetic effects of the extract and metals were evaluated by determining the total antioxidant capacity and total flavonoid/phenolic content of *S. officinalis* and NPs. DPPH scanvenging activity, BHA (65.89%), *S. officinalis*, Fe@NPs, Cu@NPs, Ag@NPs; It was evaluated as 79.57%, 72.30%, 75.81%, 81.12%. Against the metal chelating feature of EDTA; *S. officinalis* was 42.92%, Fe@NPs, Cu@NPs, Ag@NPs were 16.75%, 18.02%, 15.13%. When the results of the anticancer analysis are evaluated; It was determined that Fe@NPs decreased cell viability by 90%, Cu@NPs by ~96% and Ag@NPs by 85%. This study reports the successful synthesis of Fe@NPs, Cu@NPs, Ag@NPs with *S. officinalis* leaf extract. The results show that Fe@NPs, Cu@NPs, Ag@NPs can be used in biomedical applications.

Key words: *Salvia officinalis*, Green synthesis, Ag, Fe, Cu nanoparticles, Antibacterial activity, Antioxidant activity, Anticancer activity.

Introduction

Nanotechnology is the branch of science that allows making targeted changes by reducing substances to nano size (Turan *et al*., 2019). Nanoparticles are known as molecular structures with different surface properties in 1-100 nm sizes, which can provide important developments in several sectors, mainly in ecology, agriculture, and medical sectors (Anjum *et al*., 2016; Thipe *et al*., 2022).

The synthesis of nanoparticles attracts attention due to their physicochemical properties. Nanoparticles can be synthesized using various physical and chemical methods. Because chemical synthesis methods is toxic, dangerous, and expensive for the ecosystem, environmentally friendly (*green synthesis*) and economical production methods have been developed. For this, environmentally friendly synthesis of nanoparticles using biological materials such as plants and algae has attracted attention (Salem & Fouda, 2011; Zafar *et al*., 2019; Kanimozhi *et al*., 2022; Khan *et al*., 2024). The green synthesis method is basically based on the principle of synthesizing biomolecules such as amino acids, enzymes, proteins, carbohydrates, and secondary metabolites (phenolic substances, alkaloids, saponin, etc.) and metal ions as sealing agents that will prevent their growth and reduction. It has superior properties in many respects compared to those produced by chemical methods (Manikandan *et al*., 2017; Iqbal *et al*., 2023).

Copper/copper oxide nanoparticles are highly effective nanoparticles due to their ease of access, high electrochemical stability, tunable morphology, easy surface functionalization, and non-toxicity, as well as magnetic properties, electrical, and optical. They are also more economical than precious metals such as gold and silver (Balaji & Ilangeswaran, 2022). Iron/iron oxide nanoparticles are mainly synthesized as FeO or iron oxide types by reduction of Fe(II) containing iron salts. Magnetic FeNPs have received great attention due to their strong catalyst properties, their use in dye removal, and their effectiveness in selective applications in industry (Roy *et al*., 2021). AgNPs are among the most studied nanomaterials in the literature owing to their antibacterial, anti-inflammatory, and antioxidant effects as well as many properties such as biosynthesis, and biomedical and antimicrobial applications (Zafar *et al*., 2019; Chakravarty *et al*., 2022).

Salvia officinalis is in the class of medicinal plants of Mediterranean origin. *S. officinalis* species are known for some of their therapeutic effects, such as treating wounds and skin infections, as they contain flavonoids, phenolic acids, and terpenes, which are usually found in plants and have various therapeutic effects. *S. officinalis* stands out with its therapeutic effects including antioxidant, antibacterial and antiviral activities. It has been used in the treatment of various diseases such as heart diseases, colds, liver problems, nervous system disorders, tuberculosis, bleeding in different parts of the world (Ghaedi *et al*., 2015; Ehsani *et al*., 2021; Sabry *et al*., 2022; Ferreira *et al*., 2022).

Different environmentally friendly nanoparticles of *S. officinalis* were synthesized and their biological activities

(i.e. anticancer and antioxidant) were studied (Ghaedi 2015; Wang *et al*., 2015; Baharara *et al*., 2017; Albeladi *et al*., 2020; Abomuti *et al*., 2021; Ehsani *et al*., 2021). In this paper, the comparative properties of different metal nanoparticles under the same laboratory conditions were studied for the first time using the same *S. officinalis* aromatic medicinal plant extract. Fe, Cu and Ag nanoparticles were synthesized with the extract obtained from *S. officinalis* aromatic medicinal plant leaves. Three nanoparticles were synthesized from the same plant and the biological activities of the nanoparticles were evaluated comparatively for the first time in this study.

Material and Method

Materials: *Salvia officinalis*, $CuSO_4$ (copper (II) sulfate/Sigma-aldrich, 99-100.5% purity), $AgNO_3$ (silver nitrate/ Sigma-aldrich, 99 %purity), $FeCl_24H_2O$ (iron chloride/MERCK, Assay ≥99.0 %), $FeCl_36H_2O$ (Iron(III) chloride/ MERCK, 99.0-1002.0%), Folin-Ciocalteu Reagent (FCR/ Sigma-aldrich), Na_2CO_3 (Sodium carbonate/ Sigma-aldrich, 99-100.5% purity), Gallic acid (MERCK, Assay ≥99.0), $NaNO_2$ (Sodium nitrite/ /MERCK, Assay: 99.0-100.5 %), NaOH (Sodium hydroxide/ Sigma-aldrich, 98-100.5% purity), $AICI_3$ (Aluminum chloride), quercetin (Sigma-aldrich, ≥95% purity), DPPH (*2,2-diphenyl-1-picrylhydrazil*), ferrozine, $FeCl_2$, Sulfuric acid (H_2SO_4), Ammonium molybdate($(NH_4)_6Mo_7O_{24}.4H_2O$), Nutrient broth, Muller hintone agar, Phosphate Buffer Solution (PBS), DMEM, Fetal Serum Bovine (FBS), Trypsin, penicillin-streptomycin, DMSO (Dimethyl sulfoxide), WST-1 (*4-[3-(4-Iodophenyl)-2-(4-nitro-phenyl)-2H-5-tetrazolio]-1, 3-benzene sulfonate*).

Extraction and preparation of plant material: *Salvia officinalis* was purchased commercially. Its leaves were ground into powder. 25 g was weighed and 250 mL (1/10) of distilled water (dH_2O) was added. The prepared mixture was stirred at 40°C and 1200 rpm for 24 hours. The resulting extract was filtered through a 125 mm laboratory filter paper. *S. officinalis* leaf extract, which was filtered and particles, was used for nanoparticle synthesis (Kuppusamy *et al*., 2017).

Green synthesis of nanoparticles: For the synthesis of Fe@NPs; 1.08 g $FeCl_24H_2O$ and 0.54 g $FeCl_36H_2O$ were added to 100 mL of dH_2O, respectively, and dissolved at 60°C. 10 mL of *S. officinalis* leaf extract was added to the solution and stirred magnetically for 24 hours. The change in color of the mixture from green to brown indicated that the nanoparticle was formed.

For the synthesis of Cu@NPs; 2 g $CuSO_4$ was weighed and added to 100 mL dH_2O. Thawed at 40°C. 10 mL of *S. officinalis* extract was added. It was stirred at 1200 rpm at 40°C for 24 hours. The change in color from green to dark brown indicated that nanoparticle synthesis had occurred.

For Ag@NP synthesis; 2 g of $AgNO_3$ was added into 100 mL dH_2O, dissolved at 40°C, and 10 mL of S. officinalis extract was added. It was stirred at 1200 rpm for 24 hours. The change in the color of the extract from light brown to dark brown indicated that nanoparticle synthesis had occurred.

Fe, Cu, and Ag@NPs formed after these processes were taken to eppendorf tubes for washing. It was centrifuged at 14500 rpm for 5 minutes and the supernatant was poured, then washed 3 times with dH_2O and 2 times with ethanol. It was left at 37°C (Kaya *et al*., 2018).

Characterization of nanoparticles: Synthesized nanoparticles were characterised in terms of their morphological features such as size, shape, ionic charge, surface area using the following equipments: *X-Ray Diffraction (XRD), Zeta sizer, Transmission Electron Microscopy (TEM), Scanning Electron Microscope (SEM)/EDx, Fourier Transforms Infrared Spectroscopy (FT-IR), Dynamic light scattering method (DLS), UV-Visible*. These techniques provide important information about commercial applications of nanoparticles (Salem & Fouda, 2011).

Uv-vis spectral analysis is suitable for characterization and examination as nanoparticles have optical properties and are sensitive to agglomeration state, shape, concentration, and refractive index near the surface of nanoparticles. FT-IR spectroscopy is used to confirm the possible involvement of functional groups or biomolecules in the formation and stabilization of nanoparticles. This method produces an IR spectrum similar to a molecular fingerprint and is a powerful tool for identifying chemical bonds in a molecule. TEM is a sensitive technique that allows obtaining images at the atomic size and is used to control the morphological shape and size distribution of nanoparticles. Zetasizer, zeta potential, which is a measure of the net charge, is an indicator of the potential stability of the colloidal system. Nanoparticles repel each other if they have negative or positive potential and show high stability when the nanoparticle charge is nearly neutral. XRD is used to determine the size distribution of nanoparticles by measuring the dynamic fluctuations of light scattering intensity caused by Brownian motion. It is based on the principle of refracting X-rays in a characteristic order depending on the unique atomic arrangement of each crystal phase and is used to determine the crystal structure of nanoparticles (John *et al*., 2021). SEM is a type of electron microscope used to obtain images by scanning the sample surface with a focused beam of electrons (Sebeia *et al*., 2020).

Antioxidant activity measurement tests: Antioxidant activity measurements of nanoparticles were carried out to compare plant extract and nanoparticles. Measurements were made at 1 mg/mL concentrations of nanoparticle and extract. To prepare the nanoparticles at desired concentrations of 1 mg/mL, 10 µL of DMSO and distilled water were added and dissolved in a sonicator. Experiments were carried out in two parameters, plant extract and nanoparticle.

Determination of total antioxidant activity: The phosphomolybdenum method was used to determine the total antioxidant capacity. Evaluations were made according to Prieto & Pineda (1999). Equivalently ascorbic acid was used. 0.6 M H_2SO_4, 28 mM NaH_2PO_4 buffer and 4 mM ammonium molybdate $(NH_4)6Mo_7O_{24}.4H_2O$) solution were prepared. To prepare 0.6 M H_2SO_4 solution, 3.3 mL of H_2SO_4 was dissolved in dH_2O. To prepare 4 mM ammonium molybdate solution; 0.48 g ($(NH_4)6Mo_7O_{24}.4H_2O$) dissolved in distilled water, for 28 mM NaH_2PO_4 solution; 0.34 g of

NaH_2PO_4 was weighed and dissolved in dH_2O. The prepared solutions were combined in a bottle and dH_2O was added to make the volume 100 mL. For each sample, 25 µL of the extract solution and 250 µL of the reagent were taken and mixed. The samples were kept in a water bath at 95°C for 90 minutes, transferred to a 96-well plate, and their absorbance was measured at 695 nm on the ELISA device.

Determination of phenolic content: Total phenolic content was determined according to the Folin-Ciocalteu Reagent (FCR) method with some modifications. For FCR, 50 mL of FCR was taken, with a total volume of 100 mL, and it was covered with dH_2O. Na_2CO_3 solution was prepared by dissolving 1 g of Na_2CO_3 in 50 mL of distilled water. 100 µL of plant extract and nanoparticle solutions were taken and transferred to a 96-well plate. 100 µL of Folin-Ciocalteu solution was added, and incubated for 5 minutes, and 100 µL of sodium carbonate (20g/100 mL) was added. The total volume was completed to 300 µL. After incubation in the dark for 90 min at 25°C, gallic acid was read at 760 nm according to the standard graph, and the total phenolic content was given as gallic acid equivalent (mg GAE/g) (Hajji *et al*., 2010).

Determination of flavonoid content: The total flavonoid content was determined using the method of Estevinho *et al*., (2008). For the $NaNO_2$ solution, 7.5 g of $NaNO_2$ was dissolved in dH_2O and the total volume was made up to 50 mL. NaOH solution; 2 g of NaOH was dissolved in dH_2O and the top was completed to a volume of 50 mL. $AlCl_3$ solution; 5 g $AlCl_3$ was dissolved in dH2O, the volume was completed to 50 mL Standard quercetin solution; 5 mg of quercetin was dissolved in 5 mL of methanol. For the samples, 10 µL of extract solution was taken and transferred to 96 plates, 40 µL of distilled water and 6 µL of sodium nitrate (150 g/L) solution were added to them and left for 6 minutes after vortexing. After this process, 3 µL of aluminum chloride (2.5 g / 25 mL) was added, mixed gently and incubated for 5 minutes to equilibrate. Then, 40 µL of sodium hydroxide (4 g/100 mL) solution and 100 µL dH_2O were added, the amount was determined by vortexing and reading against quercetin as a standard in the spectrophotometer at 415 and 510 nm.

DPPH scanvenging: In order to eliminate the radical effect of DPPH, measurements were made by following the method developed by various researchers such as Hatano *et al*., (1988). In order to deactivate the radical, the extract obtained from *S. officinalis* was mixed with DPPH, and spectrophotometric reading was performed. The amount of activity was calculated according to the color removal status of the DPPH obtained as a result of the reading. 0.1 mM DPPH: 2 mg DPPH was dissolved in 100 mL Methanol. 50 µL of extract solution was taken for the samples and transferred to 96-well plates. Then, 200 µL of DPPH was added and vortexed. It was incubated for 60 minutes in the dark and measured at 517 nm. The calculation was made using the given formula:

$$\% \text{ DPPH scanvenging } (\%) = [((A_C - A_E)/ A_C) \times 100]$$

***** A_C: Absorbance of control sample
*A_E: Absorbance of the example sample

Metal chelating activity: Metal chelating activity was determined using the method of Dinis & Almeida (1994) with minor modifications. Madeira 5 mM ferrozine solution: 0.0492 g ferrozine was dissolved in 40 mL methanol. 2 mM $FeCl_2$ solution: 0.0160 g $FeCl_2.4H_2O$ was dissolved in 40 mL methanol. For each sample in turn, 50 µL of the extract solution was taken, and transferred to 96 plates, 160 µL of dH_2O and 5 µL of $FeCl_2$ (2 mM) were added and mixed by vortexing. After 30 seconds, 20 µL of ferrozine (5 mM) was added and mixed. Following this, the absorbance of the Fe^{+2}-Ferrozine mixture, which was kept at room temperature for 10 minutes, was measured at 562 nm, and the iron chelating activity of the extract was calculated using the formula given below. Metal chelating activity is expressed in EDTA equivalent (µg/mL).

$$\text{Inhibition } (\%) = [((A_C - A_E)/ A_C) \times 100]$$

***** A_C: Absorbance of control sample
*A_E: Absorbance of the example sample

Determination of antimicrobial activity: Nutrient Broth and Muller Hinton media were weighed in the amount specified in the manual and sterilized after filling with distilled water and thawing well in a magnetic stirrer. 9 mL of Nutrient Broth medium was added into glass tubes and with the help of disposable specials, stock bacteria were taken from the stock bacteria kept at +4ºC and inoculated into liquid medium. The medium then was incubated at 37°C for 24 hours. The next day, the appropriate bacterial concentration was calculated considering the Mc Farland 0.5 standard. (0.08-0.13 abs). 90 µL of Gram-positive (*Bacillus subtilis IM622, Staphylococcus aureus ATCC 29213*) and Gram-negative bacteria (*Salmonella typhimurium* NRRLE 4413, *Escherichia coli (ATCC 25922*), yeast (*Saccharomyces cerevisiae ATCC 76521*) were spread on Muller Hinton Agar. 20 mg/ml sample was aseptically impregnated into 6 mm discs in petri dishes. The antimicrobial activity of Fe, Cu, AgNps prepared with *S. officinalis* extract and the plant's own extract was determined with streptomycin, which was also used as a positive control.

***In-vitro* Anticancer Activity:** 10% (50 mL) FBS and 1% (5 mL) penicillin-streptomycin were added to a 500 mL DMEM medium. It was kept at +4 C until it was used. A549 cancer cell lines, which were kept stocked, were used. Dissolved cells in the karyotype were taken into 15 ml falcon tubes and after adding 4 ml of DMEM medium, they were centrifuged at 4500 rpm for 4 minutes, and the supernatant was discarded. 4 mL of medium was re-added to the cells and pipetage was performed. After this procedure, the cells were transferred to 25 flasks, multiplied in a 37ºC and 5% CO_2 incubator, and then used in the study.

Cell viability test: 2 mg of *S. officinalis* extract was weighed, DMEM was added at a concentration of 1 mg/mL. Experiments were carried out at different concentrations (1000, 500, 250, 125, 62.5 µg/mL). *S. officinalis* Fe, Cu, Ag@NPs were dissolved with 10 µL of DMSO and their concentration was adjusted to 2 mg/mL. A549 cancer line was taken from the stock cells and it was dissolved at 37ºC. The cells were then centrifuged at 4500

rpm for 4 min. The pellet portion was taken and 4 mL of DMEM medium was added to it. The pellet portion was transferred to a 25-gauge flask. The samples were kept in the incubator for 2 days. Afterward, the cells were counted with a thoma slide, inoculated on 96-well plates (10.000 cells per well) and after the cells were kept in the incubator for 2 days again, *S. officinalis* extract, Fe, Cu, and Ag@NPs were concentrated in different concentrations (1000, 500, 250, 125, 62.5 µg/mL) was applied. Plates were taken and examined under an inverted microscope, and the medium was applied to the cells as a control. 10 µL of WST-1 substance was added to each well. Cells were incubated for 4 hours. Then, absorbance values at 450-630 nm were taken and recorded in the ELISA reader device.

Results

Characterization of nanoparticles: Nanoparticles were synthesized using *S. officinalis* extract. The bioreduction of Fe, Cu and Ag@NPs to zerovalent metallic nanoparticles was monitored using field scanning UV-visible absorption spectrometry at 180-1100 nm wavelengths for Fe, Cu and Ag@NPs. Ag@NPs were found to form bands in the 300-400 nm range. It was observed that Fe@NPs formed bands at 270-290 nm and Cu@NPs formed bands in the range of 270-320 nm. Ag@NPs were found to form bands in the 300-400 nm range. The strong surface plasmon resonance property confirmed the presence of nanoparticles (Fig. 1A, 1B, 1C).

Characteristic peaks were recorded in XRD analyzes performed at 2θ scale. Fe@NPs; The indices corresponding to the peaks in Fig. 2A at 18°, 32°, 37°, 50°, 58°, 62° and 71° are respectively; (110), (400), (440), (200), (220) and (311). For Cu@NPs; The indices corresponding to these peaks in Fig. 2B at 27°, 32°, 38°, 44°, 46°, 54°, 57°, 64°, 77° and 81°, respectively; (110), (220), (311), (222), (400), (422), (511), (440) and (620). Ag@NPs; Fig. 2C indices corresponding to the peaks in A at 38°, 44°, 64°, 77° and 81°, respectively; (111), (200), (220), (311), (222).

FT-IR analysis was performed to determine the functional groups of nanoparticles. In the FT-IR analysis of Fe@NPs, peaks of 961, 1047, 1143, 1255, 1318, 1381, 1404, 1587, 2972, 3369 cm^{-1} values were recorded Fig. 3A. Values recorded for Cu@NPs; 501, 5180, 5705, 812, 900, 1047, 1137, 1191, 1175, 1259, 1520, 1367, 1468, 1519, 1584, 1799, 2156, 2924, 3258 cm^{-1}. Fig. 3B. For Ag@NPs, 566, 576, 845, 1010, 1154, 1316, 1415, 1474, 1508, 1537, 1603, 1713 1774, 2333, 2918 cm^{-1} values were recorded Fig. 3C.

Elements in the structure of nanoparticles were determined using the EDX method. The peaks of Fe, O and C elements were recorded in the structure of Fe@NPs Fig. 4A The peaks of the elements Cu, C and O in the structure of Cu@NPs were recorded Fig. 4B The peaks of the elements Ag and C were recorded in the structure of Ag@NPs Fig. 4C.

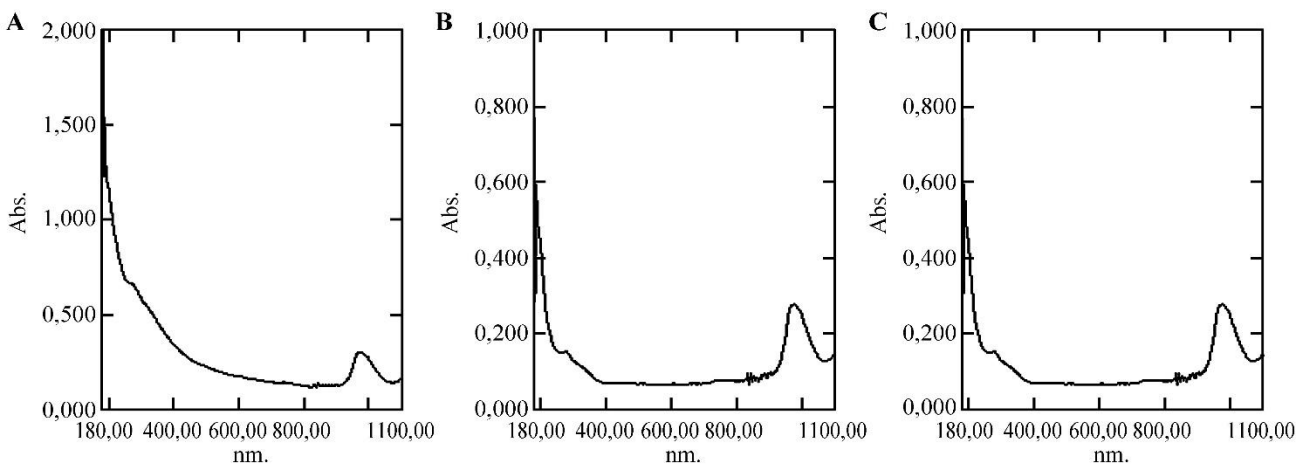

Fig. 1. Uv-vis field scanning of NPs, A: Fe@NPs, B: Cu@NPs, C:Ag@NPs.

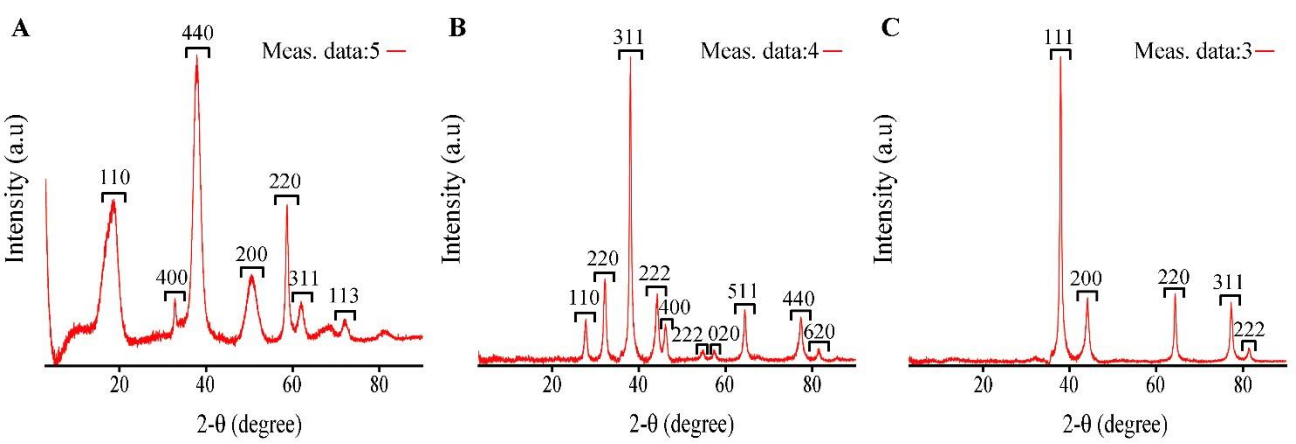

Fig. 2. XRD spectrum graph of NPs, A: Fe@NPs, B: Cu@NPs, C: Ag@NPs.

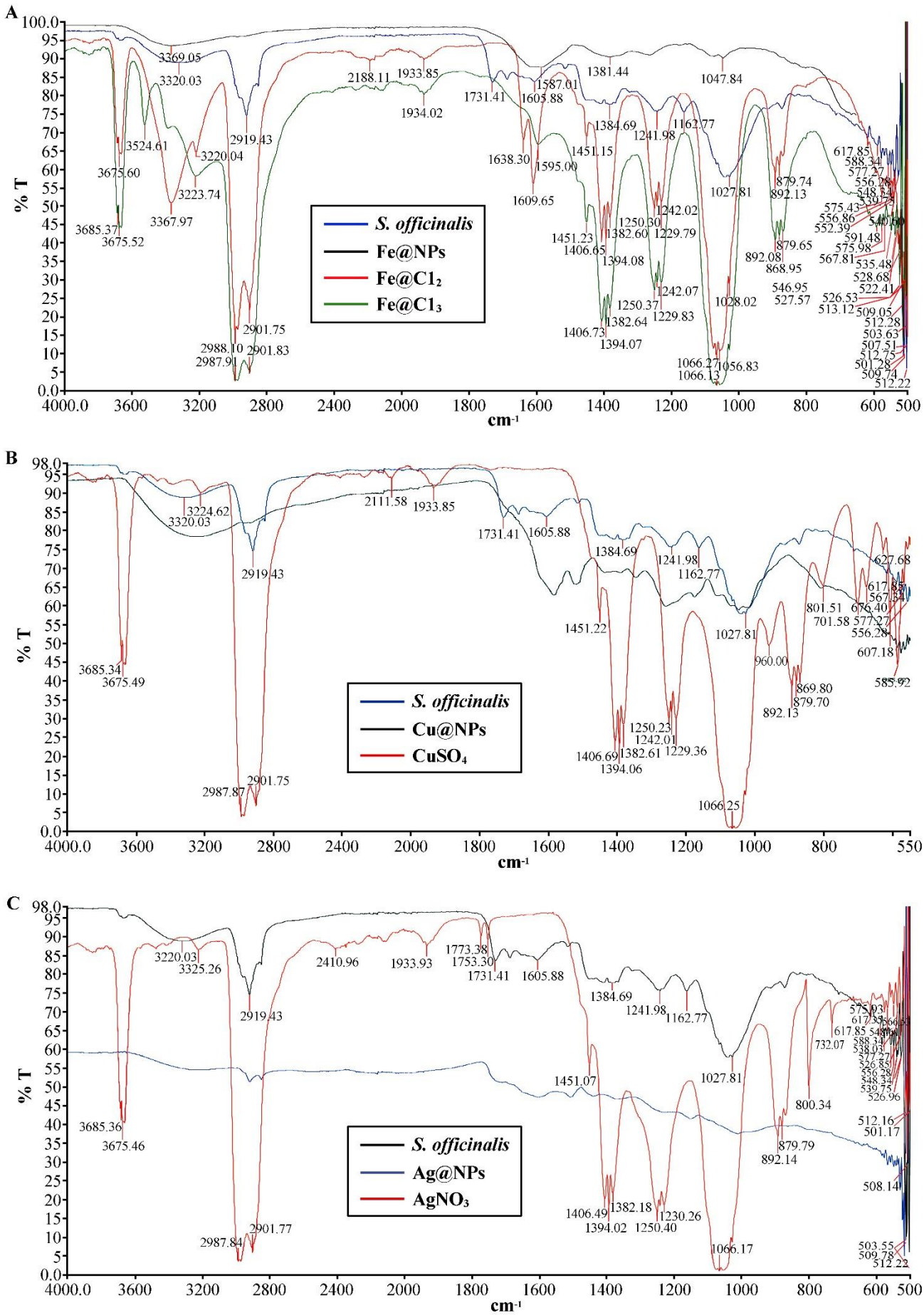

Fig. 3. FT-IR spectroscopy graph of NPs, **A:** Fe@NPs, B**:** Cu@NPs, **C:** Ag@NPs.

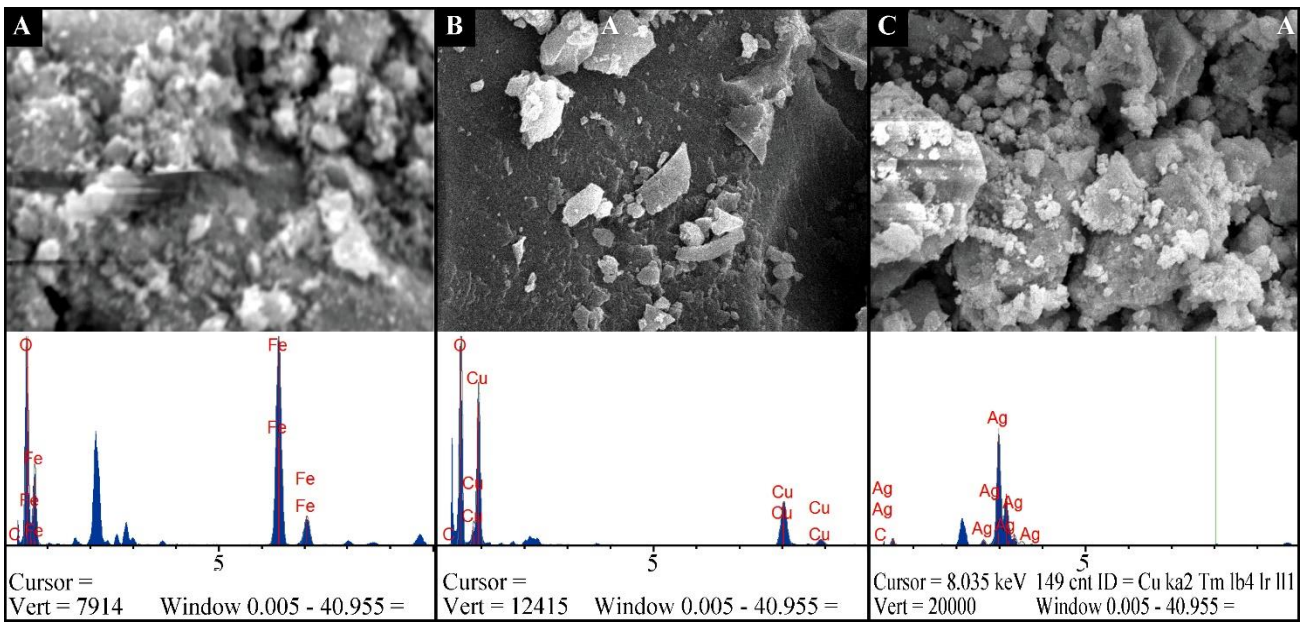

Fig. 4. EDX analysis of NPs**, A:** Fe@NPs**,** B: Cu@NPs, **C:** Ag@NPs.

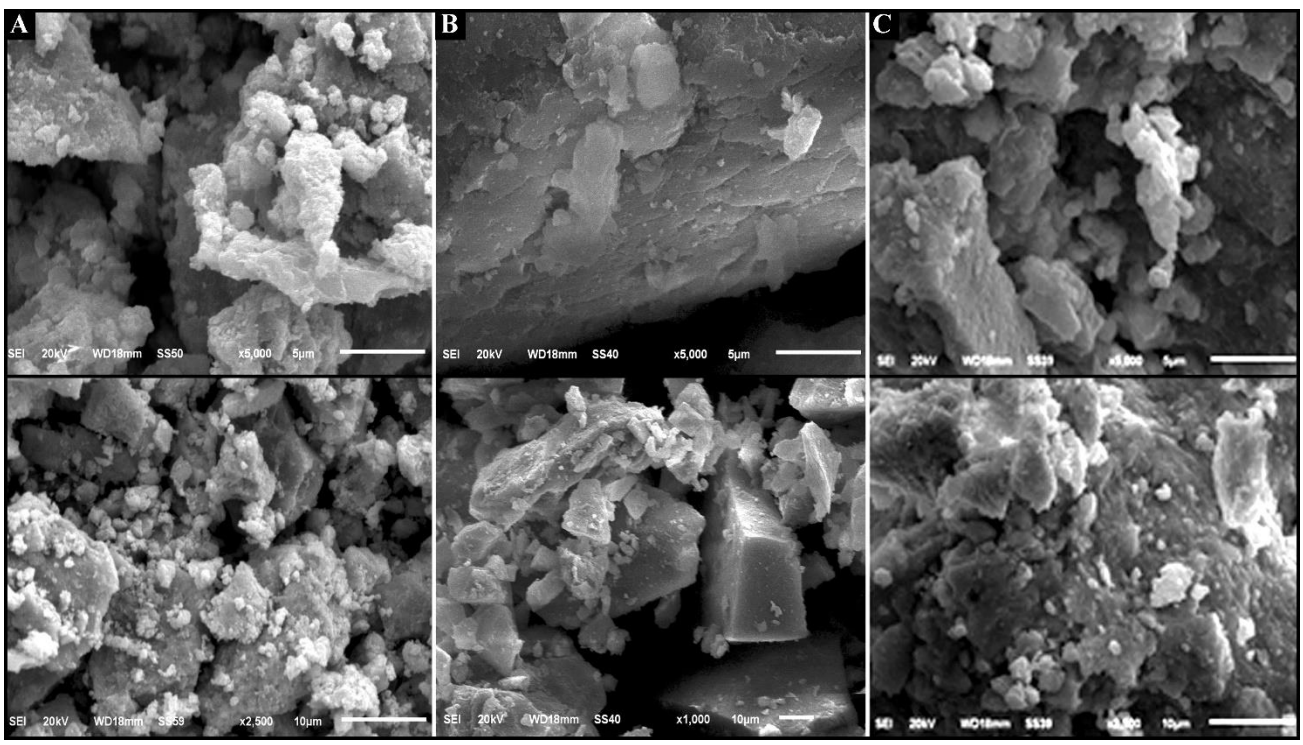

Fig. 5. Sem images of NPs, **A:** Fe@NPs, B: Cu@NPs, **C:** Ag@NPs.

When the data obtained from the SEM images were evaluated, it was observed that the morphology of Fe@NPs showed round and cubic high agglomerate tendency and closed-packed nanoparticles. SEM image of Fe@NPs is given in Fig. 5A. When the SEM image of Cu@NPs is examined in Fig. 5B, more agglomerated structures are observed, but when carefully examined, spherical nanoparticles attract attention. When SEM images of Ag@NPs were evaluated in Fig. 5C, circular structure and agglomerated structure such as Fe and Cu@NPs were observed. This agglomerated structure in NPs is thought to be due to the high surface charge and magnetization or the plant extract used as a capping/ reducing agent (Koteeswari *et al*., 2022).

Micrographs and size distribution histogram graphs obtained from TEM results of green synthesis Fe@NPs, Cu@NPs and Ag@NPs are given in (Fig. 6A, 6B, 6C).

Zeta potential provides information about the surface charge of nanoparticles and any coating or material on the surface (Parmar & Sanyal, 2022). The electrical charge of the green synthesis Fe@NPs, Cu@NPs and Ag@NPs was recorded by zeta potential analysis. Fig. 7A, 7B, 7C. It was determined as -22.2 mV for Zeta Fe@NPs, -25.5 mV for Cu@NPs and -24.6 mV for Ag@NPs.

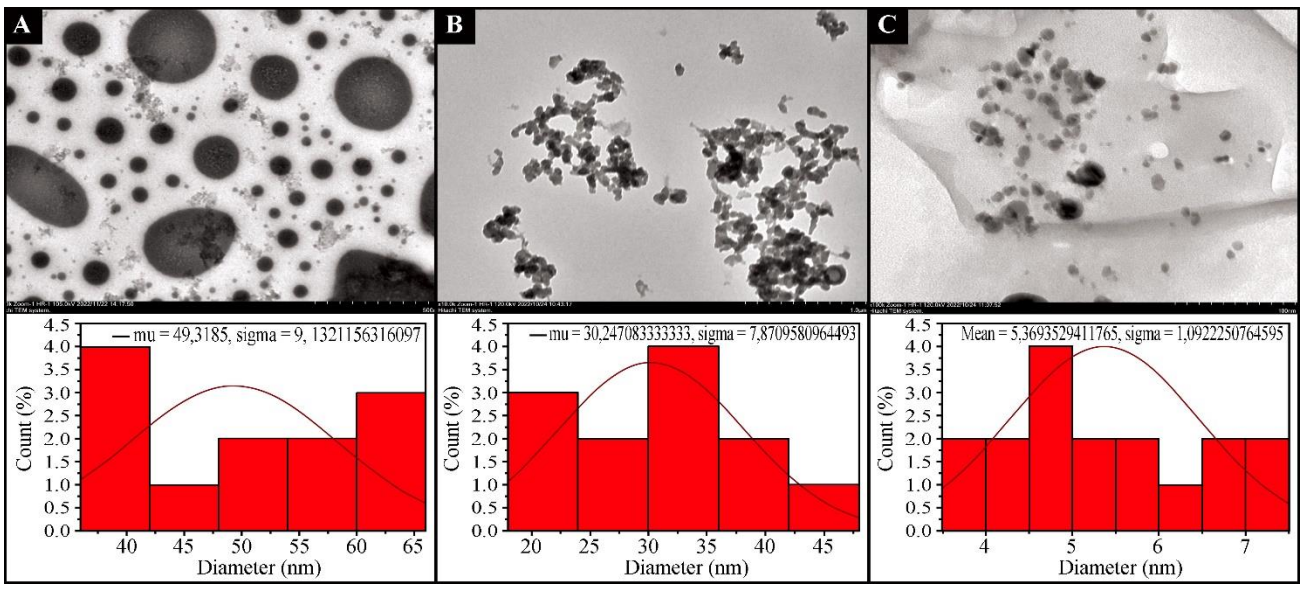

Fig. 6. TEM micrographs of NPs-size distribution histogram, A: Fe@NPs, B: Cu@NPs, C: Ag@NPs.

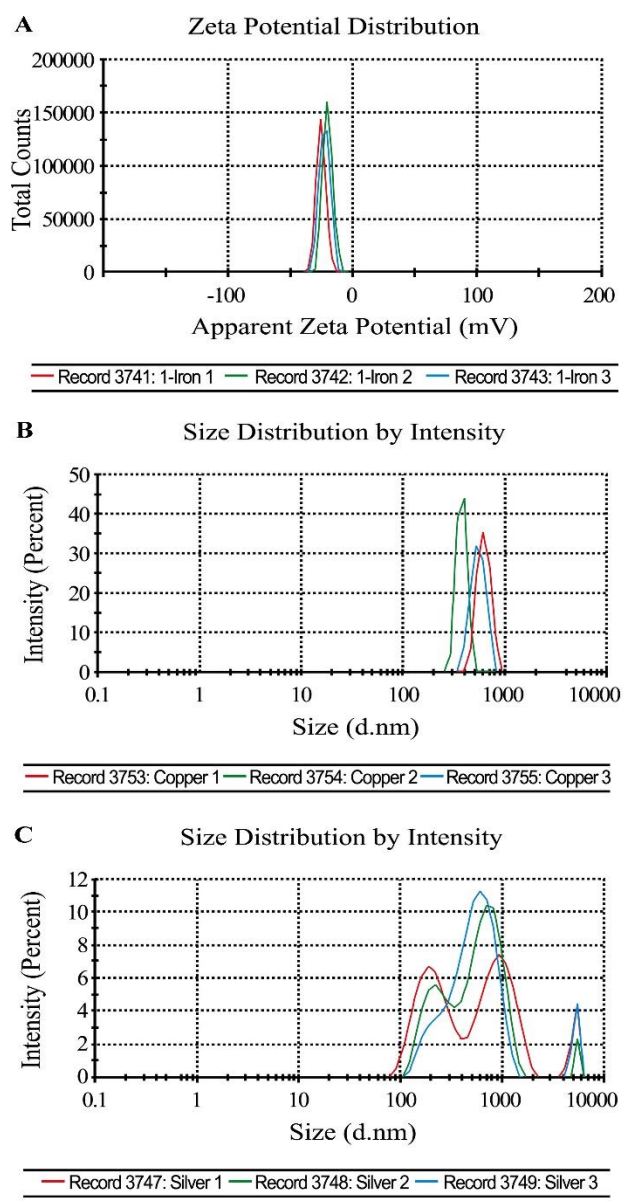

Fig. 7. Zeta potential graph of NPsA: Fe@NPs, B: Cu@NPs, C: Ag@NPs.

Antimicrobial activities of nanoparticles: In the present study, disc diffusion method was used for antimicrobial activity measurement. *S. officinalis* extract and dissolved nanoparticles were impregnated with 6 mm discs at 20 mg/mL under aseptic conditions. The antibacterial activity of *S. officinalis* extract and iron, copper, silver nanoparticles were tested using streptomycin as a positive control against gram-positive and gram-negative bacteria and yeast samples. When the antimicrobial activities of *S. officinalis* extracts were compared, it was seen that the high antimicrobial effect in *S. aureus* was also shown in other bacterial species, but this effect was relatively less (Fig. 8; Table 1). Copper nanoparticles showed the highest effect in *E. coli* iron nanoparticles, on the other hand, showed a higher effect on *S. aureus* compared to other bacteria and yeast. Silver nanoparticles showed high antimicrobial activity in both gram-negative and gram-positive bacteria (Table 1).

Anticancer analysis: A549 lung cancer cell line was used to investigate the anticancer activity of *S. officinalis* extract and Fe, Cu, Ag@NPs, and their effects on cell viability were determined *In vitro* by WST-1 assay (Fig. 9A, 9B, 9C). When *S. officinalis* extract and nanoparticles applied to A549 cancer line cells at different concentrations (1000, 500, 250, 125, 62.5 µg/mL) for 24 hours compared to control cells, it was observed that *S. officinalis* extract significantly reduced cell viability at 125 and 62.5 µg/mL concentrations. Cu@NPs were found to reduce cell viability by approximately 96% at a concentration of 62.5 µg/mL and to have an effect of 55% at 125 µg/mL. It has been noted that Fe@NPs reduce cell viability by 90% and 250 at 500 µg/mL and 95% at concentrations at 125 µg/mL. Although Ag@NPs reduced cell viability at all doses, it was determined that the highest efficiency was approximately 95% at 125 and 62.5 µg/mL, and at 250 µg/mL it reduced cell viability by approximately 85%. It was determined that cell viability decreased significantly and showed high anticancer effect at 125 and 62.5 µg/mL concentrations in all groups. Although a cytotoxic effect was noted at other doses administered, it was not found to be of high significance when compared to the control.

Total antioxidant capacity: In order to determine the total antioxidant capacity, the results are given as ascorbic acid equivalent (AA µg/g) using the phosphomolybdenum method. The antioxidant values for *S. officinalis* were determined as 3591.09 (µg/g), 3564.73 (µg/g) for Ag@NPs, 1026.55 (µg/g) for Fe@NPs and 2551.09 (µg/g) for Cu@NPs (Fig. 10).

Determination of total phenolic/Flavonoid content: *S. officinalis* total phenolic content; It was calculated as 217.266 (µg/g), Fe@NPs as 150.477, Cu@NPs as 149.193 (µg/g) and Ag@NPs as 182.954 (µg/g) (Fig. 11). Total flavonoid content of *S. Officinalis* extract; It was calculated as 36892, Fe@NPs as 26792, Cu@NPs as 23232 (µg/g), and Ag@NPs as 26832 (Fig. 12).

Determination of DPPH radical remov: As a result of spectrophotometric analyzes performed to measure radical activity, the DPPH removal activity of BHA, a synthetic antioxidant, was calculated as 65.89%. Calculated values for *S. officinalis*, Fe, Cu and Ag@NPs are; It was 79.57%, 72.30%, 75.81%, 81.12% (Fig. 13). The metal chelating capacity was evaluated based on the metal chelating property of EDTA. The metal chelating activity of *S. officinalis* extract was determined as 42.92%, while Fe, Ag, Cu@NPs were determined as 16.75%, 18.02%, 15.13% (Fig. 14).

Table 1. Disc diffusion test results (inhibition zone diameters).

Microorganism	International microorganism code	*Salvia officinalis*	Fe@NPs	Cu@NPs	Ag@NPs	Streptomycin inhibition zone (mm)
Staphylococcus aureus (gram+)	ATCC 6538P	13	10	2	10	17
Bacillus subtilis (gram+)	ATCC 6633	6	1	1	8	23
Escherichia coli (gram-)	ATCC 25922	8	1	5	5	23
Salmonella typhimurium (gram-)	CCM 5445	8	-	-	7	15
Saccharomyces cerevisiae	ATCC 9763	4	1	-	-	16

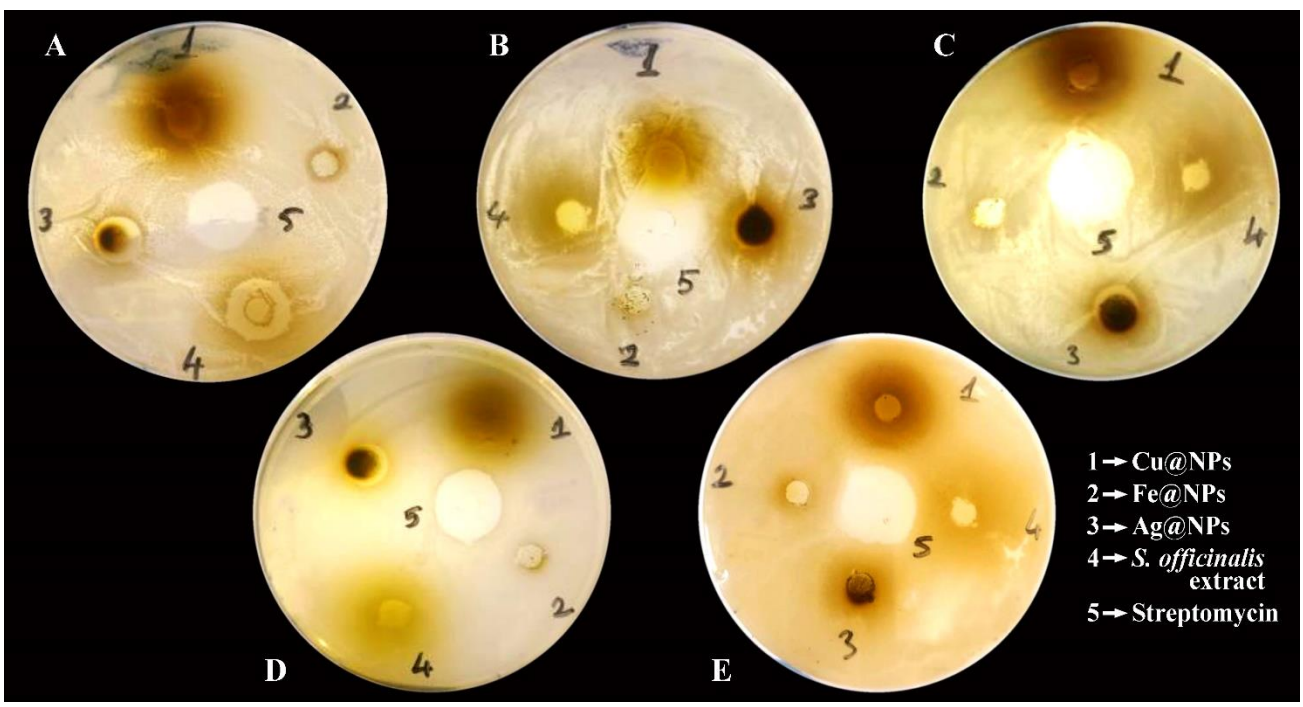

Fig. 8. Antimicrobial Activities A: *S. aureus* B: *E. coli* C: *B. subtilis* D: *S. typhimurium* E: *S. cerevisiae.*

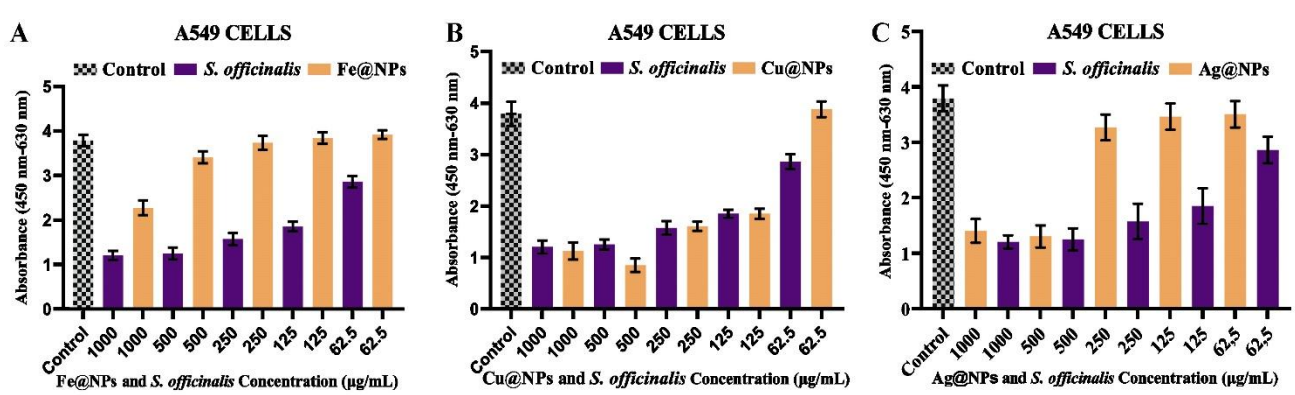

Fig. 9. Effects of NPs on A549 cell line, A: Fe@NPs, B: Cu@NPs, C: Ag@NPs.

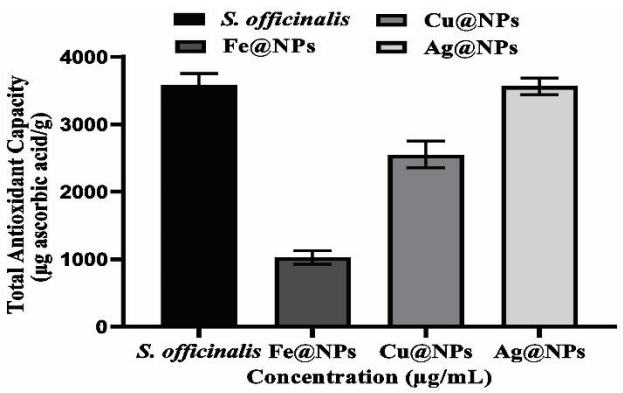

Fig. 10. Total antioxidant capacities.

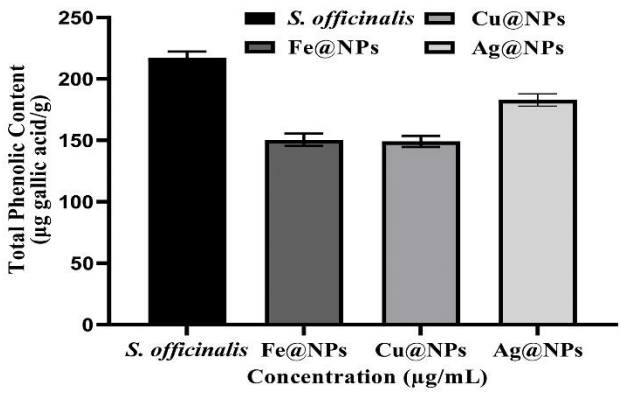

Fig. 11. Total phenolic substance content.

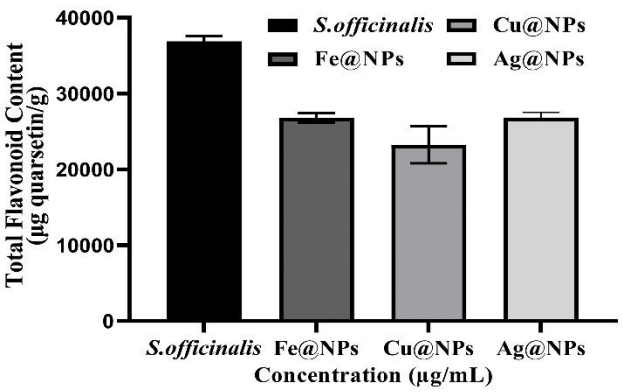

Fig. 12. Total flavonoid substance content.

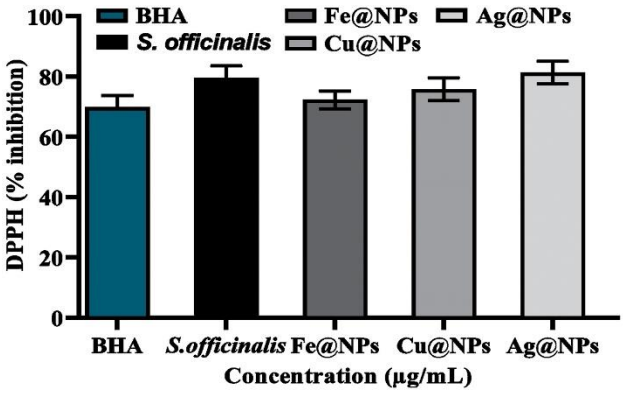

Fig. 13. % DPPH radical clearance graph of NPs.

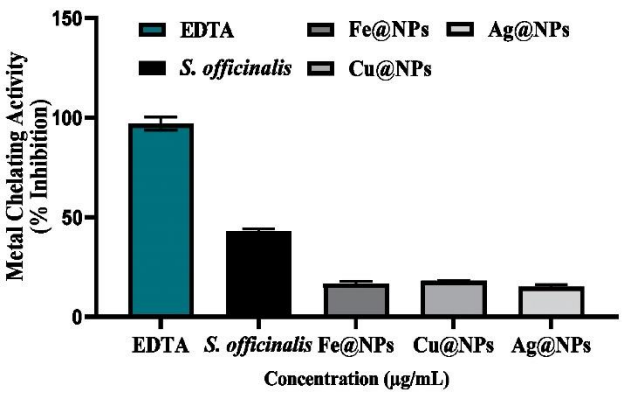

Fig. 14. % Metal chelation graph of NPs.

Discussion

Characterization of nanoparticles: Aqueous extract of *S. officinalis* is very rich in terms of flavonoid (rosmarinic acid, carnasol, rutin, etc.) content. Flavonoids in plant extracts can interact with metal ions of metal nanoparticles via bioreduction via the hydroxyl group (OH) (Sathishkumar *et al*., 2018; Albeladi *et al*., 2020). *S. officinalis* can be used as a reducing and stabilizing/coating agent in the biosynthesis of metal/metal oxide nanoparticles (Albeladi *et al*., 2020). In the present study, Fe, Cu and Ag@NPs were synthesized with *S. officinalis* and characterized using molecular techniques such as UV-vis, XRD, FT-IR, SEM, TEM. According to the UV-vis results, Fe@NPs showed an absorbance band at wavelengths of 270-290 nm and this result is consistent with previous studies. Velsankar *et al*., (2022), the absorbance band at 289 nm shows the surface plasmon resonance (SPR) band of iron oxide nanoparticles and confirms that this synthesized nanoparticle is iron oxide. Jamzad & Bidkorpeh (2020) reported that iron oxide nanoparticles synthesized with *Laurus nobilis* leaf extract show SPR bands at 285 nm. It was also reported by Karpagavinayagam & Vedhi (2019), that iron oxide nanoparticles synthesized with *Avicennia marina* flower extract exhibit SPR bands at 295-301 nm. Ag@NPs showed absorbance band at 280-300 wavelengths. Previous studies with biosynthetic AgNPs have also recorded SPR bands at different wavelengths ranging between 380 to 470 nm (Ali *et al*., 2022; Al-Mashud *et al*., 2022; Alshameri *et al*., 2022; Ganaie *et al*., 2022; Vankudoth *et al*., 2022). In the current study, band formation in the range of 270-320 nm was observed for Cu@NPs and this range is consistent with previous studies. Kolahalam *et al*., (2022), synthesized CuO nanoparticles from plant extracts of *Ocimum sanctum* and *Saussurea lappa* and reported that two absorption points were formed at approximately 270 and 500 nm. They stated that the absorption point at 270 nm is due to CuO nanoparticles and the other absorption point at 500 nm is due to components such as phenolics and flavonoids. In another study in which the characterization of biosynthetic Cu@NPs was performed, wavelengths in a wide band range of 200-800 nm were recorded. High wavelengths of Cu@NPs show that NPs have been successfully synthesized (Koteeswari *et al*., 2022). When the 2θ scale XRD analyzes of nanoparticles

were evaluated; Fe@NPs; It has been recorded that it gives characteristic peaks at 18°, 32°, 37°, 50°, 58°, 62° and 71°, and the indices corresponding to these peaks are respectively; (110), (400), (440), (200), (220) and (311). Panikar *et al*., (2022), performed XRD analyzes of biosynthetic Fe@NPs and reported characteristic peaks at 25°, 34°, 37°, 42°, 52°, 56°, 64°, 66° and 73°. Ag@NPs; Characteristic peaks were recorded at 38°, 44°, 64°, 77° and 81° and the indices corresponding to the peaks, respectively; (111), (200), (220), (311) and (222). Al-Mashud *et al*., (2022), reported that the XRD analysis results of AgNPs synthesized from *Cinnamomum tamala* aqueous leaf extract showed four strong diffraction peaks at angles of 38°, 44.1°, 64.42° and 77.46°. For Cu@NPs; Peaks were recorded at 27°, 32°, 38°, 44°, 46°, 54°, 64°, 77° and 81°. The indices corresponding to these peaks, respectively; (220), (311), (222), (400), (422), (511), (440) and (620). Kolahalam *et al*., (2022), XRD peaks of CuO NPs obtained from *Ocimum sanctum* and *Saussurea lappa* plant extract are 32.39°, 35.40°, 38.50°, 46.19°, 48.67°, 53.46°, 58.16°, 61.48°, 65.66° , 66.06°, 67.97°, 72.17° reported that it corresponds to the peaks. The presence of the substance used as the coating agent of nanoparticles can be determined by FT-IR. It was recorded in the wavelength range of 400-4000 cm^{-1}, which enables the synthesis of Fe@NPs and also some functional groups of *S. officinalis* extract. In FT-IR analysis of Fe@NPs, 961, 1047, 1143, 1255, 1318, 1381, 1404, 1587, 2972 cm^{-1} It was seen that cm-1 showed peaks of 3369 cm^{-1}. 3369 cm^{-1}–OH stretch, 1587 cm^{-1}H-O-H bond, 1255 and 1143 cm^{-1}plant material and 1381 cm^{-1}, 1404 cm^{-1}, 1587 cm^{-1}, 2972 cm^{-1} alkane groups and 961 cm^{-1} Indicates the Fe–O stretch. The presence of different molecules and functional groups indicates the formation and stabilization of the synthesized Fe@NPs (Devatha *et al*., 2018; Karpagavinayagam *et al*., 2019; Duman *et al*., 2021). For Ag@NPs, 566, 576, 845, 1010, 1154, 1316, 1415, 1474, 1508, 1537, 1603, 1713, 1774, 2333, 2918 cm^{-1} values were recorded. Two peaks thought to be compatible with the CH extensions of CH_2 functional groups (2333 cm^{-1} and 2918 cm^{-1}), which were displaced after silver biosorption in the region in the 2918 cm^{-1} range, appeared, indicating the participation of methylene groups in the process (Yang *et al*., 2017). Two peaks appeared in the region between 2800 cm^{-1} and 3000 cm^{-1} were consistent with CH extensions of CH_2 functional groups (2925 cm^{-1} and 2855 cm^{-1}), which underwent a slight displacement after silver biosorption; participation of methylene groups in the process (Yang *et al*., 2017). In the amide region (1500-1800 cm^{-1}), amide I (1603 cm^{-1}) containing C=O stretching of peptide bonds (1508, 1537, 1603, 1713 and 1774 cm^{-1}) and amide II (1537 cm^{-1}) undergo shifts after biosorption. In particular, it shows the presence of peak carbonyl groups corresponding to mobile amide II at 1508 cm-1 (Kadukova, 2016; El-Sayed & El-Sayed, 2020). Values recorded for Cu@NPs; 501, 5180, 5705, 812, 900, 1047, 1137, 1191, 1175, 1259, 1520, 1367, 1468, 1519, 1584, 1799, 2156, 2924, 3258 cm^{-1}. According to these peaks, the OH groups are due to the aromatic stretching vibration of 3258 cm^{-1} and C=C, and the peaks between 1575 cm^{-1} and 1047 cm^{-1} are due to the stretching of C=C aromatic rings and C-OH vibrations from phenolics and flavonoids (Nasrollahzadeh *et al*., 2014).

Elements in the structure of Fe, Cu and Ag@NPs were determined by the EDX method (Fig. 4A, 4B, 4C). Accordingly, the high Fe peak as seen in Fig. 4A confirms the formation of nanoparticles. The amount of oxygen in the structure of Fe@NPs indicates the presence of iron oxides. The combinations of Fe, C, and O seen in elemental analysis indicate the presence of nanoparticles as well as binding with *S. officinalis*. In addition, the presence of Fe and O confirms the high purity of Fe@NPs (Singh *et al*., 2020; Duman *et al*., 2021). The combination of Cu, C and O was observed in the elemental analysis of Cu@NPs. Sharp peaks with Cu and Os confirm the formation of Cu@NPs (Fig. 4B). The presence of oxygen with copper indicates that copper sulfate is reduced to copper oxide (Shubhashree *et al*., 2022). When EDX analyzes of Ag@NPs are evaluated, the presence of Ag and Cs can be observed (Fig. 4C). The formation of nanoparticles was confirmed by the peak of Ag at 8.035 keV (Vankudoth *et al*., 2022). When TEM micrographs of nanoparticles (Fig. 6A, 6B, 6C) were examined, it was observed that Ag@NPs are spherical in shape and 5.36 ± 1.09 nm in size. The structure of biosynthesized Ag@NPs can be clearly seen from the TEM images. The sizes of Ag@NPs are similar to previous studies (Hamedi & Shojaosadati, 2019; Al-Mashud *et al*., 2022; Ganaie *et al*., 2022). From the TEM images of Cu@NPs synthesized Ag@NPs, it was determined that the nanoparticles were in cubic shape and their dimensions were 30.24 ± 7.87 nm. The reason why nanoparticles were seen in larger sizes is considered as aggregation (Ilbasmis-Tamer *et al*., 2022). When the TEM images of Fe@NPs were examined, it was found that they had a circular structure and their dimensions were 49.31 ± 9.13 nm. Fe@NPs that are aggregates can be seen in larger sizes (Velsankar *et al*., 2022). The zeta potential analysis results of nanoparticles have determined the electrical charge of AgNPs as -24.6 mV. According to this value, Ag@NPs show a moderate stability (Raj *et al*., 2017). The zeta potentials of Cu@NPs were -25.5 mV, indicating the stability of Cu@NPs due to the increase in electrostatic repulsion forces (Ilbasmis-Tamer *et al*., 2022). The zeta potential of Fe@NPs was -22.2 mV. This value indicates the moderate stability of the nanoparticles. The reason for recording negative values proves that organic compounds adhere to the surface of NPs (Akbaba *et al*., 2017; Singh *et al*., 2020; Duman *et al*., 2021).

Antimicrobial analysis: Although different test methods and test microorganisms have been used in antimicrobial activity studies, the reliability and suitability of the Disk Diffusion method have been emphasized in many studies (Onbaşili *et al*., 2011). The antimicrobial effect of *S. officinalis* was noted in the present study. *S. officinalis* extract showed a high effect on *S. aureus* and could be considered significant in other groups. Plants such as *S. officinalis* have the ability to inactivate microbial adhesion because they have secondary metabolites. Therefore, these plants can be used as a static agent against pathogenic bacteria and fungal agents (Ghaedi *et al*., 2015). Although Cu@NPs showed an activity in all tested bacteria, they showed the highest effect in *E. coli*, which showed pathogenic properties. Our results are in agreement with the literature. It has been stated in studies that Cu@NPs can

replace gold and silver nanoparticles in many fields such as use, antimicrobial activity, antiviral, herbal production and many other fields (Husen & Siddiqi 2014; Ameh & Sayes, 2019; Chaerun *et al*., 2022). Iron nanoparticles, on the other hand, showed a higher effect on *S. aureus* compared to other bacteria and yeast. Silver nanoparticles showed high activity in both gram-negative and gram-positive bacteria. When metal/metaloxide NPs, which are seen as antimicrobial nano-agents, are evaluated, Ag@NPs draw attention due to their high antimicrobial properties and effectiveness against bacteria, viruses and fungi. Although the mechanism of action of the antibacterial activity of Ag@NPs on gram-negative (*E. coli*) and gram-positive bacteria (*S. aereus*) cannot be clearly stated, the researchers have previosly explained the antibacterial activity of Ag@NPs by associating their adhesion to the bacterial surface and destabilizing the bacterial cell wall (Tang & Zheng 2018; Crisan *et al*., 2021; Calabrese *et al*., 2022).

Anticancer analysis: Anticancer studies were performed in A549 lung cancer line cells. It was observed that *S. officinalis* aqueous extract significantly reduced cell viability at concentrations of 1000, 500 and 250 µg/mL. Natural products of plant origin are of interest as a potential source of anticancer agents. *S. officinalis* species and other plants are used in the treatment of many cancer and tumor diseases among the public (Lichota & Gwozdzinski, 2018; Adewole, 2020). *S. officinalis* has cytotoxic properties against cancer cells, it also contains severaal chemicals with antimicrobial, antioxidant and anti-inflammatory activities (Eghbaliferiz, *et al*., 2018; Najar *et al*., 2021; Karami *et al*., 2021; Yu *et al*., 2021). It has been noted that Fe, Cu and Ag@NPs significantly reduced cell viability by showing high anticancer activity at other doses and especially at concentrations of 1000, 500 and 250 µg/mL. It is known that transition metals such as Cu, Ag, Au attract attention as antibacterial and anticancer (Liu & Gust, 2016; Jakob *et al*., 2021). Nanomedicine plays an important role in realizing more effective and alternative treatment strategies for cancer (Barabadi *et al*., 2017; Yoonus *et al*., 2020). Nanoparticles produced by biological synthesis method are promising in cancer treatment because they are environmentally friendly, biocompatible and low cost. It has been reported that copper ions released by CuO NPs arrest the cell cycle in lung A549 cancer line cells. It induces DNA damage and pulls down the cell nuclear antigen (Hanagata *et al*., 2011; Preethi *et al*., 2022). FeO NPs are being studied more and more as an alternative anticancer application to reduce cytotoxicity and side effects of chemotherapy (Yusefi *et al*., 2020).

Antioxidant analysis: When antioxidant studies were evaluated, the total phenolic content of *S. officinalis* was calculated as 217.266 (µg/g), Fe@NPs 150.477, Cu@NPs 149.193 (µg/g) and Ag@NPs 182.954 (µg/g). The values of total flavonoid content were calculated as *S. officinalis* extract 36892, Ag@NPs 26832, Fe@NPs 26792 and Cu@NPs 23232 (µg/g). The strong antioxidant properties of *S. officinalis* species have also been reported in other studies. It has been reported that *S. officinalis* plant has biological properties such as antioxidant, antitumor and antibacterial due to its richness in phenolic and volatile compounds. The reason why plants are rich in these compounds is interpreted as the substitution of natural plant defense mechanisms and a possible ecological intensification of agriculture (Stagos *et al*., 2012; Garcia *et al*., 2016; Bahadori *et al*., 2018; Khiya *et al*., 2019). Khiya *et al*., (2019), at the end of his study with *S. officinalis*; states that polyphenols, catechics, and flavonoids are intensely present in *S. officinalis*. It reports that it is rich in phenolic content (1.044 ± 0.004 mg GAE/g extract) and flavonoids (0.037 ± 0.003 mg EQ/g extract). The DPPH radical is stable because the spare electron is delocalized on the molecule and prevents dimer formation. The dark purple color disappears when DPPH is reduced to its non-radical form by antioxidants. The model system of DPPH radicals is widely used to investigate the scavenging behavior of various natural compounds. When the DPPH radical is scavenged, the color of the reaction mixture changes from purple to yellow with decreasing absorbance at 517 nm (Thakar *et al*., 2021). Calculated values for *S. officinalis*, Cu, Fe and Ag@NPs in the present study; 79.57%, 75.81%, 72.30%, 81.12%. Biosynthesis Ag@NPs showed the highest DPPH removal. This shows that it can have a synergistic effect when combined with *S. officinalis*. Thakar *et al*. (2021), stated in their study that CuONPs synthesized with the leaf extract of *Cissus vitiginea* plant have higher antioxidant activity than the plant extract and are closer to ascorbic acid, which is used as a standard. Dose-dependent CuONPs showed significant inhibition of DPPH activity compared to *Cissus vitiginea* leaf extract. Kanchana *et al*. (2022), reported that biosynthesized Ag@NPs are good radical scavengers. He states that Ag@NPs act as hydrogen or electron donor in the conversion of the DPPH radical to its reduced form. Ag@NPs act against up to 80.44 DPPH free radicals at 100 µg/mL (Saratale *et al*., 2018; Saratale *et al*., 2019; Kanchana *et al*., 2022. Abdullah *et al*., (2020), reported that the total antioxidant activities of biosynthesis Fe_2O_3 and Fe_3O_4 NPs are high. He recorded the highest and lowest values of the different nanoparticle concentrations as 180 mg EAG/g NPs (0.01 M NPs) and 77 mg EAG/g NPs (0.03 M), respectively, and this is the relationship between concentration and antioxidant activity. evaluated that the degree of inhibition of both DPPH and total antioxidant activity at low concentrations is much higher than at high concentration. Zakariya *et al*., (2022), reported that biosynthesis Fe@NPs showed strong antioxidant activity. Compared with ascorbic acid, the IC_{50} values of 12.2 µg/mL of Fe@NPs indicate that they exhibit a high potential against the DPPH radical and can be used as antimicrobial, anticancer agents in the future. The metal chelating capacity was evaluated against the metal chelating property of EDTA. The metal chelating activity of EDTA was calculated as 97.66%. On the other hand, *S. officinalis* extract was determined as 42.92% and Ag, Fe, Cu@NPs were determined as 15.13%, 16.75%, 18.02%.

Conclusion

The extract obtained from the *S. officinalis* plant was used as a reducing and coating agent and environmentally friendly Fe, Cu, and Ag@NPs were synthesized, their characterization was determined using molecular such as UV-vis, FT-IR, XRD, SEM, EDX, TEM and Zeta

potential. The results prove that the nanoparticles were successfully synthesized. Antimicrobial, anticancer and antioxidant tests of synthesized NPs were performed. Nanoparticles in antioxidant analysis; total antioxidant capacities, DPPH radical scavenging efficiency, metal chelating effect, phenolic and flavonoid capacities were evaluated and antioxidant capacities were found to be high. A549 lung cancer line cells were used in cell culture studies of nanoparticles and the effect of nanoparticles on these cells was investigated. As a result of the research, it was determined that *S. officinalis* extract and biosynthesis nanoparticles, which showed activity at all concentrations, showed higher efficiency at lower concentrations. The results show that biosynthesis nanoparticles can efficiently provide efficacy in many fields. In addition, considering that the studies conducted are *In vitro*, it shows that these studies should also be evaluated as *In vivo*.

Acknowledgements

This study was carried out within the scope of 100/2000 YÖK doctoral scholarship.

References

Abdullah, J.A.A., L. Salah Eddine, B. Abderrhmane, M. Alonso-González, A. Guerrero and A. Romero. 2020. Green synthesis and characterization of iron oxide nanoparticles by *pheonix dactylifera* leaf extract and evaluation of their antioxidant activity. *Sustain. Chem. Pharm*., 17: 100280.

Abomuti, M.A., E.Y. Danish, A. Firoz, N. Hasan and M.A. Malik. 2021. Green synthesis of zinc oxide nanoparticles using *salvia officinalis* leaf extract and their photocatalytic and antifungal activities. *Biology*, 10(11): 1075.

Adewole, K.E. 2020. Nigerian antimalarial plants and their anticancer potential: A review. *J. Integr. Med*., 18(2): 92-113.

Akbaba, H., U. Karagöz, Y. Selamet and A.G. Kantarcı. 2017. Synthesis and characterization of cationic lipid coated magnetic nanoparticles using multiple emulsions as microreactors. *J. Magn. Magn. Mater.*, 426: 518-524.

Albeladi, S.S.R., M.A. Malik and S.A. Al-Thabaiti. 2020. Facile biofabrication of silver nanoparticles using *Salvia officinalis* leaf extract and its catalytic activity towards Congo red dye degradation. *J. Mater. Res. Technol*., 9(5): 10031-10044.

Ali, F., U. Younas, A. Nazir, F. Hassan, M. Iqbal, B. Hamza, S. Mukhtar, A. Khalid and A. Ishfaq. 2022. Biosynthesis and characterization of silver nanoparticles using strawberry seed extract and evaluation of their antibacterial and antioxidant activities. *J. Saudi Chem. Soc.*, 26(6): 101558.

Al-Mashud, M.A., M. Moinuzzaman, M.S. Hossain, S. Ahmed, G. Ahsan, A. Reza, R.B.A. Anwar, M.H. Uddin, M.A. Momin and M.A.H.M. Jamal. 2022. Green synthesis of silver nanoparticles using *Cinnamomum tamala* (Tejpata) leaf and their potential application to control multidrug resistant *Pseudomonas aeruginosa* isolated from hospital drainage water. *Heliyon*, 8(7): 1-9.

Alshameri, A.W., M. Owais, I. Altaf and S. Farheen. 2022. *Rumex nervosus* mediated green synthesis of silver nanoparticles and evaluation of its *In-vitro* antibacterial, and cytotoxic activity. *OpenNano*, 8: 100084.

Ameh, T. and C.M. Sayes. 2019. The potential exposure and hazards of copper nanoparticles: a review. *Environ. Toxicol. Pharmacol.*, 71: 103220.

Anjum, S., B.H. Abbasi and Z.K. Shinwari. 2016. Plant-mediated green synthesis of silver nanoparticles for biomedical applications: Challenges and opportunities. *Pak. J. Bot.*, 48(4): 1731-1760.

Bahadori, M.B., M. Eskandani, D.M. Mieri, M. Hamburger and H. Nazemiyeh. 2018. Anti-proliferative activity-guided isolation of clerodermic acid from *Salvia nemorosa* L.: Geno/cytotoxicity and hypoxia-mediated mechanism of action. *Food Chem. Toxicol.*, 120: 155-163.

Baharara, J., R. Tayebeh, M. Marzieh and A.S. Majid. 2017. Antioxidant and anti-inflammatory activity of green synthesized silver nanoparticles using *Salvia officinalis* extract. *Ann. Trop. Med. Public Health*, 10(5): 1265-1270.

Balaji, R. and D. Ilangeswaran. 2022. Choline chloride–Urea deep eutectic solvent an efficient media for the preparation of metal nanoparticles. *J. Indian Chem. Soc*., 99(5): 100446.

Barabadi, H., M. Ovais. Z.K. Shinwari and M. Saravanan. 2017. Anti-cancer green bionanomaterials: Present status and future prospects. *Green Chem. Lett. Rev.*, 10(4): 285-314.

Calabrese, C., V.L. Parola, M.L. Testa and L.F. Liotta. 2022. Antifouling and antimicrobial activity of Ag, Cu and Fe nanoparticles supported on silica and titania. *Inorganica Chim. Acta*, 529: 120636.

Chaerun, S.K., B.A. Prabowo and R. Winarko. 2022. Bionanotechnology: The formation of copper nanoparticles assisted by biological agents and their applications as antimicrobial and antiviral agents. *Environ. Nanotechnol. Monit. Manag*., 18: 100703.

Chakravarty, A., I. Ahmad, P. Singh, Sheikh, M.U.D., M., G. Aalam, S. Sagadevan and S. Ikram. 2022. Green synthesis of silver nanoparticles using fruits extracts of *Syzygium cumini* and their bioactivity. *Chem. Phys. Lett.*, 795: 139493.

Crisan, M.C., T. Mocan, M. Manolea, L.I. Lasca, F.A. Tăbăran and L. Mocan. 2021. Review on silver nanoparticles as a novel class of antibacterial solutions. *Appl. Sci*., 11(3): 1120.

Devatha, C.P., K. Jagadeesh and M. Patil. 2018. Effect of green synthesized iron nanoparticles by *Azardirachta Indica* in different proportions on antibacterial activity. *Environ. Nanotechnol. Monit. Manag.*, 9: 85-94.

Dinis, T.C.P., V.M.C. Madeira and L.M. Almeida. 1994. Action of phenolic derivatives (*acetaminophen, salicylate, and 5-aminosalicylate*) as inhibitors of membrane lipid peroxidation and as peroxyl radical scavengers. *Arch. Biochem. Biophys.*, 315(1): 161-169.

Duman, S., B. Kaya, F. Caf, B. Enez and S.A. Fincan. 2021. Innovative hydrogen release from sodium borohydride hydrolysis using biocatalyst-like Fe_2O_3 nanoparticles impregnated on *Bacillus simplex* bacteria. *Int. J. Hydrog. Energy*, 46(29): 15410-15430.

Eghbaliferiz, S., S.A. Emami, Z.T. Najaran, M. Iranshahi, A. Shakeri, J. Hohmann and J. Asili. 2018. Cytotoxic diterpene quinones from *Salvia tebesana Bunge*. *Fitoterapia*, 128: 97-101.

Ehsani, P., M.R. Farahpour, M. Mohammadi, S. Mahmazi and S. Jafarirad. 2021. Green fabrication of ZnO/magnetite-based nanocomposite-using *Salvia officinalis* extract with antibacterial properties enhanced infected full-thickness wound. *Colloids Surf. A Physicochem. Eng. Asp*., 628: 127362.

El-Sayed, M.T. and A.S.A. El-Sayed. 2020. Tolerance and mycoremediation of silver ions by *Fusarium solani*. *Heliyon*, 6.5.

Estevinho, L., A.P. Pereira, L. Moreira, L.G. Dias and E. Pereira. 2008. Antioxidant and antimicrobial effects of phenolic compounds extracts of Northeast Portugal honey. *Food Chem. Toxicol*., 46(12): 3774-3779.

Ferreira, C.S.R., B.H.F. Saqueti, P.D.S. dos Santos, J.M. da Silva, M.A. Matiucci, A.C. Feihrmann, J.M.G. Mikcha and O.O. Santos. 2022. Effect of *Salvia (Salvia officinalis)* on the oxidative stability of salmon hamburgers. *LWT*, 154: 112867.

Ganaie, S.A., I. Zahoor and R. Singh. 2022. *Prunella vulgaris* leaf extract assisted green synthesis of silver nanoparticles: Antimicrobial activity. *Mater. Today: Proc*., 79(1): 107-112.

Garcia, C.S.C., C. Menti, A.P.F. Lambert, T. Barcellos, S. Moura, C. Calloni, C.S. Branco, M. Salvador, M. Roesch-Ely and J.A.P. Henriques. 2016. Pharmacological perspectives from brazilian *Salvia officinalis* (Lamiaceae): Antioxidant, and antitumor in mammalian cells. *An. Acad. Bras. Cienc.*, 88(1): 281-292.

Ghaedi, M., R. Naghiha, R. Jannesar, N. Dehghanian, B. Mirtamizdoust and V. Pezeshkpour. 2015. Antibacterial and antifungal activity of flower extracts of *Urtica dioica*, *Chamaemelum nobile* and *Salvia officinalis*: Effects of Zn $[OH]_2$ nanoparticles and Hp-2-minh on their property. *J. Ind. Eng. Chem*., 32: 353-359.

Hajji, M., R. Jarraya, I. Lassoued, O. Masmoudi, M. Damak and M. Nasri. 2010. GC/MS and LC/MS analysis, and antioxidant and antimicrobial activities of various solvent extracts from *Mirabilis jalapa* tubers, *Process Biochem*, 45(9): 1486-1493.

Hamedi, S. and S.A. Shojaosadati. 2019. Rapid and green synthesis of silver nanoparticles using *Diospyros lotus* extract: Evaluation of their biological and catalytic activities. *Polyhedron*, 171: 172-180.

Hanagata, N., F. Zhuang, S. Connolly, J. Li, N. Ogawa and M. Xu. 2011. Molecular responses of human lung epithelial cells to the toxicity of copper oxide nanoparticles inferred from whole genome expression analysis. *ACS Nano*, 5(12): 9326-9338.

Hatano, T., H. Kagawa, T. Yasuhara and T. Okuda. 1988. Two new flavonoids and other constituents in licorice root: their relative astringency and radical scavenging effects. *Chem. Pharm. Bull*., 36(6): 2090-2097.

Husen, A. and K.S. Siddiqi. 2014. Phytosynthesis of nanoparticles: Concept, controversy and application. *Nanoscale Res. Lett*., 9: 1-24.

Ilbasmis-Tamer, S., E.S. Saral-Acarca, S. Tort, Ç. Yücel, U. Tamer and F. Acartürk. 2022. Fabrication and characterization of starch-copper nanoparticles/rutin nanofiber hybrid scaffold. *J. Drug Deliv. Sci. Technol.*, 72: 103401.

Iqbal, M., N.I. Raja, S.A. Khan, A. Ali, A. Hanif, M. Hussain, T. Anwar, H. Qureshi, M. Saeed, A. Rauf, S.A. Alharbi, M.J. Ansari and R.K. Iqbal. 2023. Evaluation of green synthesized silver nanoparticles against bacterial pathogenic strains of plants. *Pak. J. Bot.*, 55(5): 1967-1972.

Jakob, C.H.G., A.W. Muñoz, J.F. Schlagintweit, V. Weiß, R.M. Reich, S.A. Sieber, J.D.G. Correia and F.E. Kühn. 2021. Anticancer and antibacterial properties of trinuclear Cu(I), Ag(I) and Au(I) macrocyclic NHC/urea complexes. *J. Organomet. Chem.*, 932: 121643.

Jamzad, M. and M.K. Bidkorpeh. 2020. Green synthesis of iron oxide nanoparticles by the aqueous extract of *Laurus nobilis* L. leaves and evaluation of the antimicrobial activity. *J. Nanostructure Chem.*, 10: 193-201.

John, M.S., J.A. Nagoth, M. Zannotti, R. Giovannetti, A. Mancini, K.P. Ramasamy, C. Miceli and S. Pucciarelli. 2021. Biogenic synthesis of copper nanoparticles using bacterial strains isolated from an antarctic consortium associated to a psychrophilic marine ciliate: Characterization and potential application as antimicrobial agents. *Mar. Drugs*, 19(5): 263.

Kadukova, J. 2016. Surface sorption and nanoparticle production as a silver detoxification mechanism of the freshwater alga *Parachlorella kessleri*. *Bioresour. Technol.*, 216: 406-413.

Kanchana, P., V. Hemapriya, N. Arunadevi, S.S. Sundari, I.M. Chung and M. Prabakaran. 2022. Phytofabrication of silver nanoparticles from *Limonia acidissima* leaf extract and their antimicrobial, antioxidant and its anticancer prophecy. *J. Indian Chem. Soc.*, 99(10): 100679.

Kanimozhi, S., R. Durga, M. Sabithasree, A.V. Kumar, A. Sofiavizhimalar, A.A. Kadam, R. Rajagopal, R. Sathya and N.I.W. Azelee. 2022. Biogenic synthesis of silver nanoparticle using *Cissus quadrangularis* extract and its *In vitro* study. *J. King Saud Univ. Sci.*, 34(4): 101930.

Karami, F., A.D. Yazdi, I. Salahshourifar and M.M. Beigi. 2021. Investigating the effects of *Salvia chorassanica bunge* and shoot extracts on gastric cancer cells: Evidence of different behavior on various tumor grades. *Pharm. Sci.*, 27(3): 378-384.

Karpagavinayagam, P. and C. Vedhi. 2019. Green synthesis of iron oxide nanoparticles using *Avicennia marina* flower extract. *Vacuum*, 160: 286-292.

Kaya, B., E. Darendelioğlu, G. Dervişoğlu and M. Tartık. 2018. Determination of comparative biological activities of silver nanoparticles formed by biological synthesis using *Achillea vermicularis. Pak. J. Bot*., 50(4): 1423-1432.

Khan, M.A., M. Khan, R. Naeem and M. Hafeez. 2024. Synergistic effect of citrus sinensis (orange) and *Aloe barbadensis* (Aloe vera) extracts on biosynthesis and antimicrobial activities of zinc oxide nanoparticles. *Pak. J. Bot*., 56(4): 1373-1378.

Khiya, Z., M. Hayani, A. Gamar, S. Kharchouf, S. Amine, F. Berrekhis, A. Bouzoubae, T. Zair and F. El Hilali. 2019. Valorization of the *Salvia officinalis* L. of the Morocco bioactive extracts: Phytochemistry, antioxidant activity and corrosion inhibition. *J. King Saud Univ. Sci.*, 31(3): 322-335.

Kolahalam, L.A., K.R.S. Prasad, P.M. Krishna, N. Supraja and S. Shanmugan. 2022. The exploration of bio-inspired copper oxide nanoparticles: synthesis, characterization and in-vitro biological investigations. *Heliyon*, 8.(6): e09726

Koteeswari, P., S. Sagadevan, I. Fatimah, A.K. Sibhatu, S.I.A. Razak, E. Leonard and T. Soga. 2022. Green synthesis and characterization of copper oxide nanoparticles and their photocatalytic activity. *Inorg. Chem. Commun.*, 144: 109851.

Kuppusamy, P., S. Ilavenil, S. Srigopalram, G.P. Maniam, M.M. Yusoff, N. Govindan and K.C. Choi. 2017. Treating of palm oil mill effluent using *Commelina nudiflora* mediated copper nanoparticles as a novel bio-control agent. *J. Clean. Prod.*, 141: 1023-1029.

Lichota, A. and K. Gwozdzinski. 2018. Anticancer activity of natural compounds from plant and marine environment. *Int. J. Mol. Sci.*, 19(11): 3533.

Liu, W. and R. Gust. 2016. Update on metal N-heterocyclic carbene complexes as potential anti-tumor metallodrugs. *Coord. Chem. Rev*., 329: 191-213.

Manikandan, V., P. Velmurugan, J.H. Park, W.S. Chang, Y.J. Park, P. Jayanthi and B.T. Oh. 2017. Green synthesis of silver oxide nanoparticles and its antibacterial activity against dental pathogens. *3 Biotech*, 7(72): 1-9.

Najar, B., G. Mecacci, V. Nardi, C. Cervelli, S. Nardoni, F. Mancianti, V.V. Ebani, S. Giannecchini and L. Pistelli. 2021. Volatiles and antifungal–antibacterial–antiviral activity of south African *Salvia* spp. Essential oils cultivated in uniform conditions. *Molecules*, 26(9): 2826.

Nasrollahzadeh, M., S.M. Sajadi and M. Khalaj. 2014. Green synthesis of copper nanoparticles using aqueous extract of the leaves of *Euphorbia esula* L., and their catalytic activity for ligand-free Ullmann-coupling reaction and reduction of 4-nitrophenol. *RSC Adv.*, 4(88): 47313-47318.

Onbaşili, D., E.M. Altuner and G.Y. Çelik. 2011. Antimicrobial activity of *Mnium marginatum* extracts. *KUOFD.*, 11(2): 205-208.

Panikar, S., A.U.R. Nanthini, V.R. Umapathy, C. SumathiJones, A. Mukherjee, P. Prakash and T.H. Farooq. 2022. Morphological, chemoprofile and soil analysis comparison of *Corymbia citriodora* (Hook.) K.D. Hill and L.A.S. Johnson along with the green synthesis of iron oxide nanoparticles. *J. King Saud. Univ. Sci.*, 34(5): 102081.

Parmar, M. and M. Sanyal. 2022. Extensive study on plant mediated green synthesis of metal nanoparticles and their application for degradation of cationic and anionic dyes. *Environ. Nanotechnol. Monit. Manag.*, 17: 100624.

Preethi, D.R.A., S. Prabhu, V. Ravikumar and A. Philominal. 2022. Anticancer activity of pure and silver doped copper oxide nanoparticles against A549 cell line. *Mater. Today Commun.*, 33: 104462.

Prieto, P., M. Pineda and M. Aguilar. 1999. Spectrophotometric quantitation of antioxidant capacity through the formation of a phosphomolybdenum complex: Specific application to the determination of vitamin E. *Anal. Biochem*., 269(2): 337-341.

Raj, A., P. Shah and N. Agrawal. 2017. Dose-dependent effect of silver nanoparticles (AgNPs) on fertility and survival of *Drosophila*: An *In vivo* study. *PLoS One*, 12(5): e0178051.

Roy, S.D., K.C. Das, and S.S. Dhar. 2021. Conventional to green synthesis of magnetic iron oxide nanoparticles; its application as catalyst, photocatalyst and toxicity: A short review. *Inorg. Chem. Commun*., 134: 109050.

Sabry, M.M., R.F. Abdel-Rahman, S.M. El-Shenawy, A.M. Hassan and S.H. El-Gayed. 2022. Estrogenic activity of *Sage* (*Salvia officinalis* L.) aerial parts and its isolated ferulic acid in immature ovariectomized female rats. *J. Ethnopharmacol.*, 282: 114579.

Salem, S.S. and A. Fouda. 2011. Green Synthesis of metallic nanoparticles and their prospective biotechnological applications: An overview. *Biol. Trace Elem. Res.*, 199: 344-370.

Saratale, R.G., G.D. Saratale, C. Si-Kyung, G. Ghodake, A. Kadam, S. Kumar, S.I. Mulla, K.Dong-Su, J. Byong-Hun, C.J. Shu and S. Han-Seung. 2019. Phyto-fabrication of silver nanoparticles by *Acacia nilotica* leaves: Investigating their antineoplastic, free radical scavenging potential and application in H_2O_2 sensing. *J. Taiwan Inst. Chem. Eng.*, 99: 239-249.

Saratale, R.G., H.S. Shin, G. Kumar, G. Benelli, G.S. Ghodake, Y.Y. Jiang, D.S. Kim and G.D. Saratale. 2018. Exploiting fruit byproducts for eco-friendly nanosynthesis: *Citrus* × *clementina peel* extract mediated fabrication of silver nanoparticles with high efficacy against microbial pathogens and rat glial tumor C6 cells. *Environ. Sci. Pollut. Res.*, 25: 10250-10263.

Sathishkumar P., F.L. Gu, Q. Zhan, T. Palvannan and A.R.M. Yusoff. 2018. Flavonoids mediated 'Green' nanomaterials: a novel nanomedicine system to treat various diseases-current trends and future perspective. *Mater. Lett.*, 210: 26-30.

Sebeia, N., M. Jabli, A. Ghith and T.A. Saleh. 2020. Eco-friendly synthesis of *Cynomorium coccineum* extract for controlled production of copper nanoparticles for sorption of methylene blue dye. *Arab. J. Chem.*, 13(2): 4263-4274.

Shubhashree, K.R., R. Reddy, A.K. Gangula, G.S. Nagananda, P.K. Badiya, S.S. Ramamurthy, P. Aramwit and N. Reddy. 2022. Green synthesis of copper nanoparticles using aqueous extracts from *Hyptis suaveolens* (L.). *Mater. Chem. Phys*., 280: 125795.

Singh, K., D.S. Chopra, D. Singh and N. Singh. 2020. Optimization and ecofriendly synthesis of iron oxide nanoparticles as potential antioxidant. *Arab. J. Chem.*, 13(12): 9034-9046.

Stagos, D., N. Portesis, C. Spanou, D. Mossialos, N. Aligiannis, E. Chaita, C. Panagoulis, E. Reri, L. Skaltsounis, A.M. Tsatsakis and D. Kouretas. 2012. Correlation of total polyphenolic content with antioxidant and antibacterial activity of 24 extracts from Greek domestic *Lamiaceae species. Food Chem. Toxicol.*, 50(11): 4115-4124.

Tang, S. and J. Zheng. 2018. Antibacterial activity of silver nanoparticles: Structural effects. *Adv. Healthc. Mater.*, 7(13): 1701503.

Thakar, M.A., S.S. Jha, K. Phasinam, R. Manne, Y. Qureshi and V.V.H. Babu. 2021. X ray diffraction (XRD) analysis and evaluation of antioxidant activity of copper oxide nanoparticles synthesized from leaf extract *of Cissus vitiginea*. *Mater. Today: Proc*., 51(1): 319-324.

Thipe, V.C., A.R. Karikachery, P. Çakılkaya, U. Farooq, H.H. Genedy, N. Kaeokhamloed, D.H. Phan, R. Rezwan, G. Tezcan, E. Roger and K.V. Katti. 2022. Green nanotechnology an innovative pathway towards biocompatible and medically relevant gold nanoparticles. *J. Drug Deliv. Technol.*, 70: 103256.

Turan, N.B., H.S. Erkan, G.O. Engin and M.S. Bilgili. 2019. Nanoparticles in the aquatic environment: Usage, properties, transformation and toxicity, A review. *Process Saf. Environ. Prot*., 130: 238-249.

Vankudoth, S., S. Dharavath, S. Veera, N. Maduru, R. Chada, P. Chirumamilla, C. Gopu and S. Taduri. 2022. Green synthesis, characterization, photoluminescence and biological studies of silver nanoparticles from the leaf extract of *Muntingia calabura*. *Biochem. Biophys. Res. Commun.*, 630: 143-150.

Velsankar, K., G. Parvathy, S. Mohandoss, G. Ravi and S. Sudhahar. 2022. *Echinochloa frumentacea grains* extract mediated synthesis and characterization of iron oxide nanoparticles: A greener nano drug for potential biomedical applications. *J. Drug Del. Sci. Tech*., 76: 103799.

Wang, Z., C. Fang and M. Mallavarapu. 2015. Characterization of iron-polyphenol complex nanoparticles synthesized by *Sage (Salvia officinalis*) leaves. *Environ. Technol. Inno.*, 4: 92-97.

Yang, Y., M. Hu, D. Zhou, W. Fan, X. Wang and M. Huo. 2017. Bioremoval of Cu^{2+} from CMP wastewater by a novel copper-resistant bacterium *Cupriavidus gilardii* CR3: characteristics and mechanisms. *RSC Adv*., 7(30): 18793-18802.

Yoonus, J., R. Resmi and B. Beena. 2020. Evaluation of antibacterial and anticancer activity of green synthesized iron oxide (α-Fe_2O_3) nanoparticles. *Mater. Today: Proc.*, 46(8): 2969-2974.

Yu, M., I. Gouvinhas, J. Rocha and A.I.R.N.A. Barros. 2021. Phytochemical and antioxidant analysis of medicinal and food plants towards bioactive food and pharmaceutical resources. *Sci. Rep*., 11(1): 10041.

Yusefi, M., K. Shameli, R.R. Ali, S.W. Pang and S.Y. Teow. 2020. Evaluating anticancer activity of plant-mediated synthesized iron oxide nanoparticles using *Punica granatum fruit peel* extract. *J. Mol. Struct.*, 1204: 127539.

Zafar, H., I.U. Haq, S. Nasreen and M. Zia. 2019. Toxicological effect of CuO nanoparticles to *brassica nigra* L. seedlings: A comparative *In vivo* and *In vitro* response. *Pak. J. Bot.*, 51(2): 427-434.

Zakariya, N.A., S. Majeed and W.H.W. Jusof. 2022. Investigation of antioxidant and antibacterial activity of iron oxide nanoparticles (IONPS) synthesized from the aqueous extract of *Penicillium spp. Sens. Int*., 3: 100164.

(Received for publication 20 October 2023)